Hindawi Publishing Corporation
International Journal of Photoenergy
Volume 2015, Article ID 376202, 8 pages
http://dx.doi.org/10.1155/2015/376202

Research Article

Luminance Conversion Property of Er and Yb Doped $KZnF_3$ Nanocrystal Synthesized by Hydrothermal Method

Weidong Lai,[1] Xinzheng Li,[2] Lu Han,[1] Huiqing Liu,[1] Yingjuan Chen,[1] Pingguang Duan,[1] and Xiaowei Li[1]

[1]*Hebei Key Lab of Optic-Electronic Information and Materials, College of Physics Science and Technology, Hebei University, Baoding 071002, China*
[2]*Department of Sciences, Hebei University of Science and Technology, Shijiazhuang 050018, China*

Correspondence should be addressed to Weidong Lai; laiwd@hbu.edu.cn

Received 17 October 2014; Accepted 17 December 2014

Academic Editor: Mohammad Muneer

In order to make full use of exposure energy, one feasible way is to modify the luminance of crystal by rare earth doping technique. $KZnF_3$:Er^{3+} and $KZnF_3$:Er^{3+}/Yb^{3+} nanocrystals of uniform cuboid perovskite type morphology, with average diameter of 130 nm, has been synthesized by hydrothermal method. When Yb^{3+} ions were codoped with Er^{3+}, absorption peak at 970 nm has been heightened and widened, and the photon absorption cross section increased. The common xenon lamp exposure cannot initiate obvious nonlinear phenomenon of the doped Er^{3+} and Yb^{3+}, and exposing at 245 nm only excites the fluorescence around 395 nm. Contrarily, under high power IR exposure at 980 nm, obvious upconversion photoluminescence (PL) has been observed due to the two-photon process. The PL mechanism of the doped Er^{3+} ion in KZnF3:Er^{3+}/Yb^{3+} nanocrystals is confirmed. Furthermore, Yb^{3+} codoped as sensitizer has modified the PL intensity of Er^{3+} from green light range to red range, and the primary channel is changed from $^4S_{3/2}(Er^{3+}) \rightarrow {}^4I_{15/2}(Er^{3+})$ of only Er^{3+} doped $KZnF_3$ nanocrystal to $^4F_{9/2}(Er^{3+}) \rightarrow {}^4I_{15/2}(Er^{3+})$ of Er^{3+}/Yb^{3+} codoped sample. With exposure energy increasing, such primary transition channel after two-photon excitation is unchanged.

1. Introduction

Since display issues have been receiving extensive attention, the photoluminescence (PL) technology based on inorganic, organic, or microcrystalline properties has developed rapidly [1]. For such a purpose, the rare earth doping technique has been investigated during recent years and was applied in many areas such as phosphors, display monitors, X-ray imaging, lasers, amplifiers for fiber-optic communication, and biological fluorescence labeling [2–7]. Among these techniques, an important research topic has attracted much attention which makes full use of exposure energy, especially converting near-infrared (NIR) irradiation into visible light, due to the easy acquirement of low-cost and high-power NIR laser diodes nowadays. Erbium cation (Er^{3+}) doped materials have been well studied, which can convert NIR exposure energy for different usages [8]. Obregóna and Colón reported that Er^{3+} doping has enhanced the photocatalytic activity of TiO_2 under sun-like excitation, acting in different energy conversion mechanisms under UV or NIR excitation, and verified the upconversion contribution of Er^{3+} ion [9]. Xin et al. doped $NaGdF_4$:Er^{3+} crystal in glass matrix and tuned the upconversion emission intensity by changing the Er^{3+} concentration, which has potential usage for the silicon solar cells [10]. It has been verified and accepted that the upconversion process is nonlinear, in which a photon at shorter wavelength is emitted after continuously absorbing more than one longer wavelength photon by long-lived intermediate energy state of lanthanide rare earth ions (Tm^{3+}, Ho^{3+}, and Er^{3+}), usually as two-photon or even three-photon excitation reactions [11]. However, restricted by the dipole-forbidden intra-4*f* transition, the photon absorption cross section of Er^{3+} is relatively small.

To enhance the upconversion efficiency, auxiliary methods have been put forward. Aisaka et al. present that upconversion PL obtains more benefits from the metal-enhanced fluorescence technique than the downconversion PL, due

to strong enhancement of upconversion photoluminescence in visible range by placing Er^{3+} near rough Ag islands in Al_2O_3 films [12]. Zhang et al. also find such enhancement in Au 3-dimensional (3D) nanostructures. Surface plasmon resonances have improved the photon absorption efficiency [13]. In such a meaning, sensitizers can also achieve improvement of photon absorption cross section. For example, the ytterbium ions (Yb^{3+}) can collect the pumping light and transfer the energy to Er^{3+} ions to participate in further upconversion [14, 15].

Except for the above stated photon absorption aspect, the substrate, in which Er^{3+} and other ions are doped, also has nonignorable influence on the upconversion efficiency. Oxide or fluoride thin films have been usually selected as substrates. The phonon energy is lower in fluoride film than oxide one, which can decrease the nonradiative loss in multiphonon relaxation and then obtain a high quantum efficiency of the desired luminescence [16–18]. Fluoride film can be synthesized by solid phase reaction or sol-gel process, but the former has oxidation problem, and the latter is difficult to perform.

In this paper, the $KZnF_3$ fluoride nanocrystals, doped by Er^{3+} and sensitizer Yb^{3+}, are synthesized by hydrothermal method. In order to clarify the modification of upconversion mechanism, the Yb^{3+} is set at 2% mole ratio, with the Er^{3+} at 0.5%. The nanocrystal diameter is 130 nm. Such fluoride substrate for upconversion was not reported thoroughly. The luminance excited at 980 nm has been observed with blue shift compared to the exciting wavelength. Upconversion has been achieved. In order to explore the luminance conversion effects, the morphology of $KZnF_3$ nanocrystal, the absorption, reflection, and FT-IR spectra and the PL spectra are characterized. Meanwhile, the mechanism of luminance conversion is discussed in this paper.

2. Experimental

2.1. Preparation of Er and Yb Doped $KZnF_3$ Nanocrystal. Rare earth oxides Er_2O_3 (99.9%, Guangfu) and hydrous chloride $YbCl_3{\cdot}6H_2O$ (99.99%, Alfa Aesar) are selected as the doping ingredients without further purification. K_2CO_3 (99.9%), ZnF_2 (99.5%), and NH_4HF_2 (99.9%) are used to synthesize substrate. The Er^{3+} doping concentration of 0.5% mole ratio and the Yb^{3+} doping as $(1-x)K_2CO_3 \cdot xYbCl_3$ ($x = 0, 2\%$) are mixed in 15 mL H_2O. The pH is adjusted at 3.

After the preparation procedure, the mixture is sealed in reactor. Then, hydrothermal method is put forward. Since crystallization can be generated in high-temperature aqueous solutions under high vapor pressures, the reaction is operated at 180°C for 30 h. The resultants are filtrated and preserved in room temperature for 10 days. Finally, the XRD, SEM, and spectra technique are employed.

2.2. Characterization of Er and Yb Doped $KZnF_3$ Nanocrystal. The crystallinity of the prepared nanocrystal is analyzed by XRD (XRD6000, Shimadzu, Japan) with Cu K_α radiation ($\lambda = 0.154056$ nm) at 40 kV and 25 mA, under scanning rate of 10°/min. The nanocrystal morphology is observed by SEM (FEI-quanta-200F, FEI, Netherlands) and Particle Size Analyzers (Zetasizer NANO ZS90, Malvern, United Kingdom). The absorption/reflection spectra, FT-IR spectra, and common fluorescence spectra are detected by UV-visible spectrometer (U-4100, Hitachi, Japan), FT-IR spectrophotometer (Tensor27, Bruker, Germany), and fluorescence spectrometer (F-4600, Hitachi, Japan), respectively. To investigate the luminance conversion property, photoluminescence (PL) emission spectra are measured using photoluminescence spectrophotometer (Fluorolog-3-TAU, Horiba Jobin Yvon, France), with the exposure source irradiated at 980 nm. All analyses were done at room temperature.

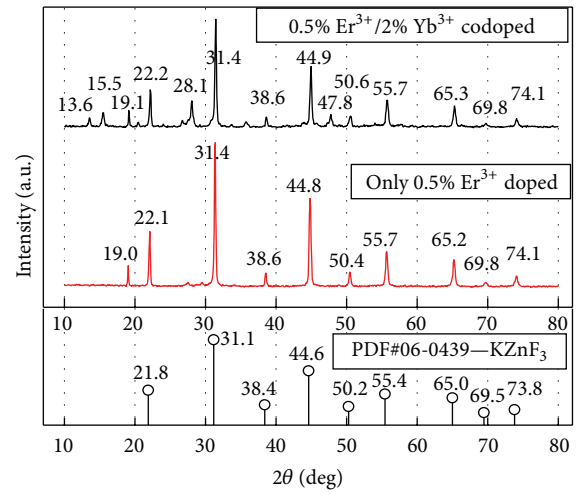

FIGURE 1: X-ray diffraction pattern of the Er^{3+}, Er^{3+}/Yb^{3+} doped nanocrystals and the standard $KZnF_3$ XRD card.

3. Results and Discussion

3.1. XRD Analysis. Phase identification of nanocrystals is performed via X-ray diffraction shown in Figure 1. X-ray diffraction pattern of the nanocrystals is matched well with the standard pattern of PDF#06-0439, which suggested that the material has crystallized as $KZnF_3$ structure.

There is a minute location increase of the diffraction peaks compared to the standard $KZnF_3$ pattern, and it can be ascribed that the diameters of the doped Er^{3+} and Yb^{3+} ions are different from the substituted ions in $KZnF_3$ crystal lattice. In addition, some additional weak peaks, such as the peaks appearing at 19.0 degrees in only Er^{3+} doped material and 13.6, 15.5, 19.1, 28.1, and 47.8 degrees of Er^{3+}/Yb^{3+} doped nanocrystals, might belong to the incompletely reacted fluoride raw materials, unwanted oxide, or oxy-fluoride impurities.

3.2. SEM and Diameter Distribution Analysis. The SEM graph is shown in Figure 2. The nanocrystal has cuboid perovskite type structure with smooth surface. Such structure can be used as optical substrate, since many ions possessing different valence states can be doped into its crystal lattice.

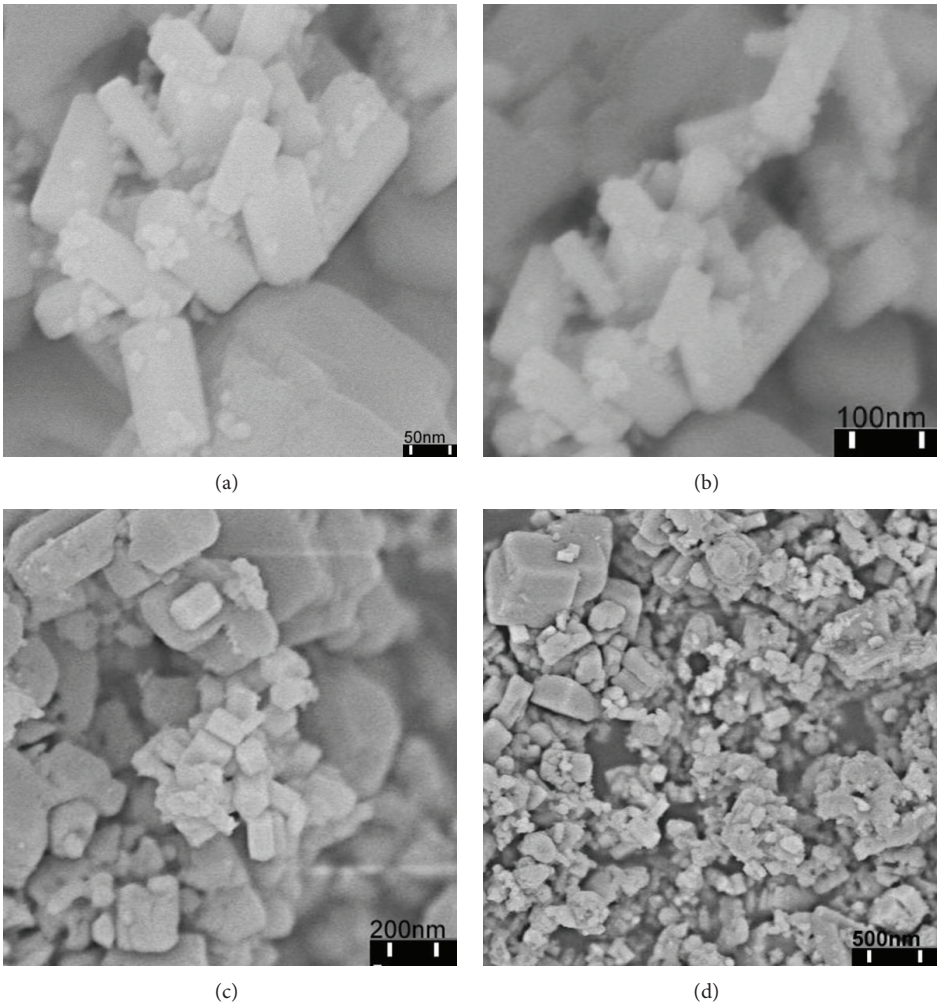

Figure 2: SEM graph of the synthesized nanocrystals.

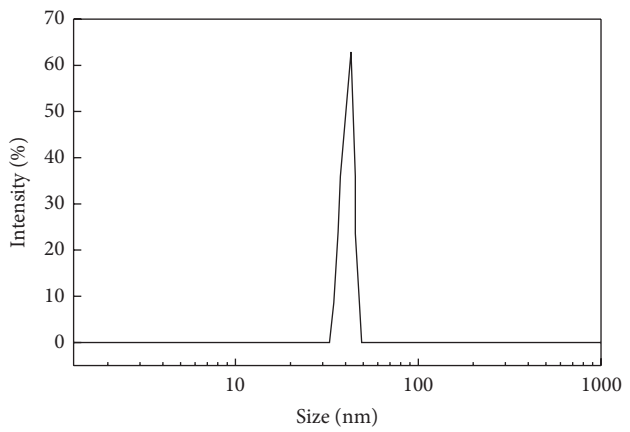

Figure 3: Diameter distribution of the synthesized nanocrystals.

The size statistics are presented in Figure 3. The average diameter of the nanocrystals is about 130 nm and has a narrow distribution, which is an advantage to realize homogeneous optical property.

3.3. UV-Vis and FT-IR Analysis. To clarify the luminance conversion mechanism, the raw materials of Er_2O_3 and $YbCl_3$ are investigated in Figures 4(a) and 4(b) by reflection and absorption spectra. Two reagents have absorption peak around 974 and 970 nm, respectively. The molecular Er_2O_3 has more absorption bands present in Figure 4(a) than the $YbCl_3$ in Figure 4(b). And the ZnF_2 only has long wavelength absorption band.

After $KZnF_3$ crystallization, narrow absorption peak around 970 nm appeared for only Er^{3+} doped material, but the absorption intensity is relatively low. When 2% Yb^{3+} ions were codoped with Er^{3+}, the absorption peak has been heightened and the absorption band has been widened, as shown in Figures 4(c) and 4(d) in reflection and absorption spectra. This suggests that the Yb^{3+} can increase the photon absorption efficiency based on its higher photon absorption cross section.

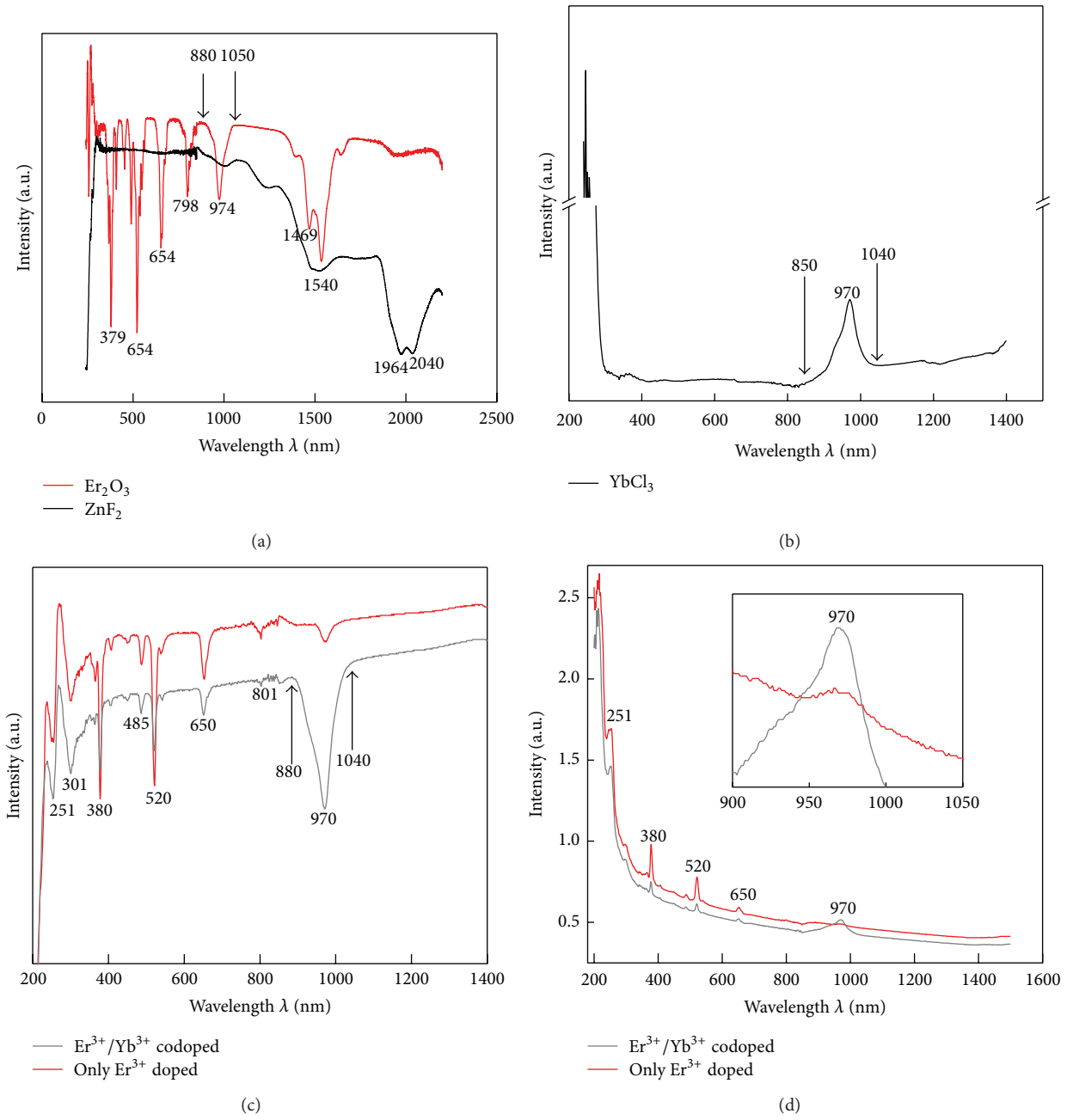

FIGURE 4: (a) Reflection spectra of Er_2O_3 and ZnF_2; (b) absorption spectra of $YbCl_3$; (c) reflection and (d) absorption spectra of Er^{3+} doped, Er^{3+}/Yb^{3+} codoped nanocrystals.

The FT-IR spectra are shown in Figure 5. The spectra peak positions are similar between the only Er^{3+} doped and the Er^{3+}/Yb^{3+} codoped samples. But the highest peak is different. The Er^{3+}/Yb^{3+} codoped nanocrystal has the highest absorbance at 748 cm^{-1}, whereas the highest absorbance of only Er^{3+} doped sample is around 420 cm^{-1}.

This result qualitatively indicates that Yb^{3+} ions can easily form chemical bonds when doped into the $KZnF_3$ nanocrystal lattice.

3.4. Luminance Spectra Analysis with Common Exposure Source. With common xenon lamp as exposure source, monitored at 490 nm, the excitation spectra have one peak at 245 nm in Figure 6(a), which is related to the transition channel of Er^{3+}:

$$^2I_{15/2}\left(Er^{3+}\right) \longrightarrow {}^2I_{11/2}\left(Er^{3+}\right). \quad (1)$$

Further exposed to irradiation of 245 nm, the emitted fluorescence is similar between the only Er^{3+} doped and Er^{3+}/Yb^{3+} codoped nanocrystals in Figure 6(b). The emission peak appears at 395 nm with a band from 350 to 550 nm.

The exposure energy of common xenon lamp is very low, and no nonlinear phenomenon appeared, even if the UV excitation at 245 nm has been employed.

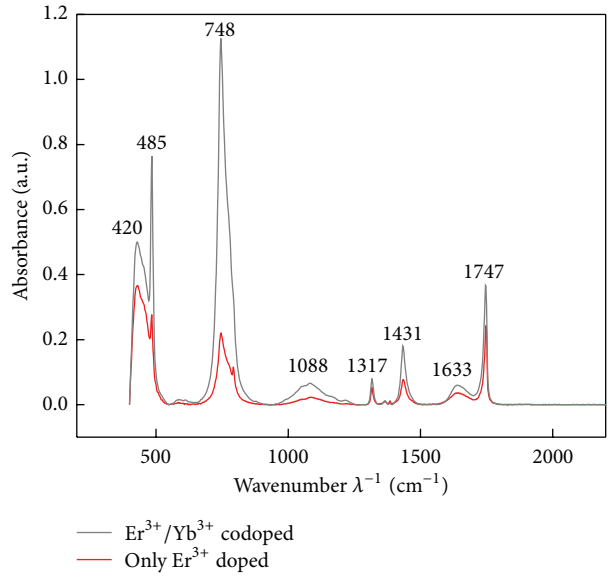

FIGURE 5: FT-IR spectra of Er^{3+} and Er^{3+}/Yb^{3+} doped nanocrystals.

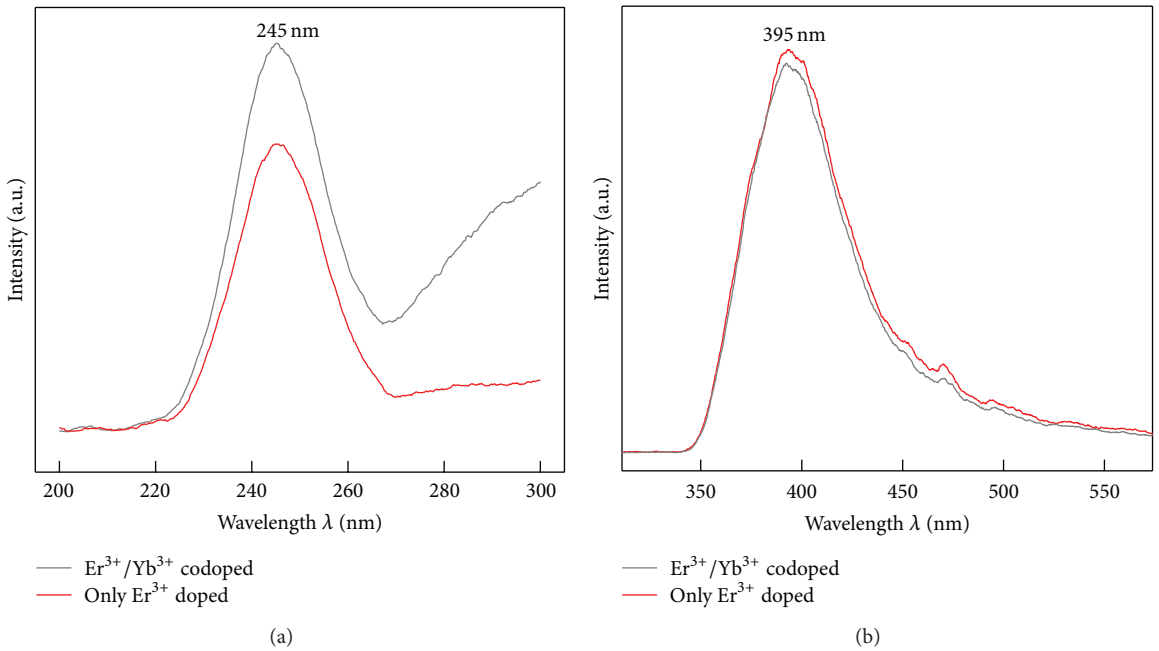

FIGURE 6: (a) Excitation and (b) emission spectra of the nanocrystal exposed to common xenon lamp.

3.5. PL Spectra Analysis under 980 nm Laser Exposure. When exposed to 980 nm laser with its energy adjusted in the scale of 50–200 mW, the emitted luminance can be directly observed by naked eyes. Fluorescence of the prepared $KZnF_3:Er^{3+}$ and $KZnF_3:Er^{3+}/Yb^{3+}$ nanocrystals in the wavelength region of 350–750 nm is shown in Figures 7(a) and 7(b), respectively. The luminance has blue shifted compared to the exposing wavelength of 980 nm. PL upconversion has been achieved for both only Er^{3+} doped and Er^{3+}/Yb^{3+} codoped $KZnF_3$ nanocrystals.

Several similar distinct emission bands are observed for the two kinds of samples, centered around 653, 539, 528, 484, and 407 nm. These emissions are ascribed to the doped Er^{3+} ions. The relationship between PL luminance peak and transition channel of Er^{3+} is shown in Table 1.

The differences of the only Er^{3+} doped and Er^{3+}/Yb^{3+} codoped nanocrystals are laid on the PL intensity. The blue PL at 407 and 377 nm are relatively low for only Er^{3+} doped nanocrystal, and such emission peaks even disappear for Er^{3+}/Yb^{3+} codoped nanocrystal. In green and red PL band,

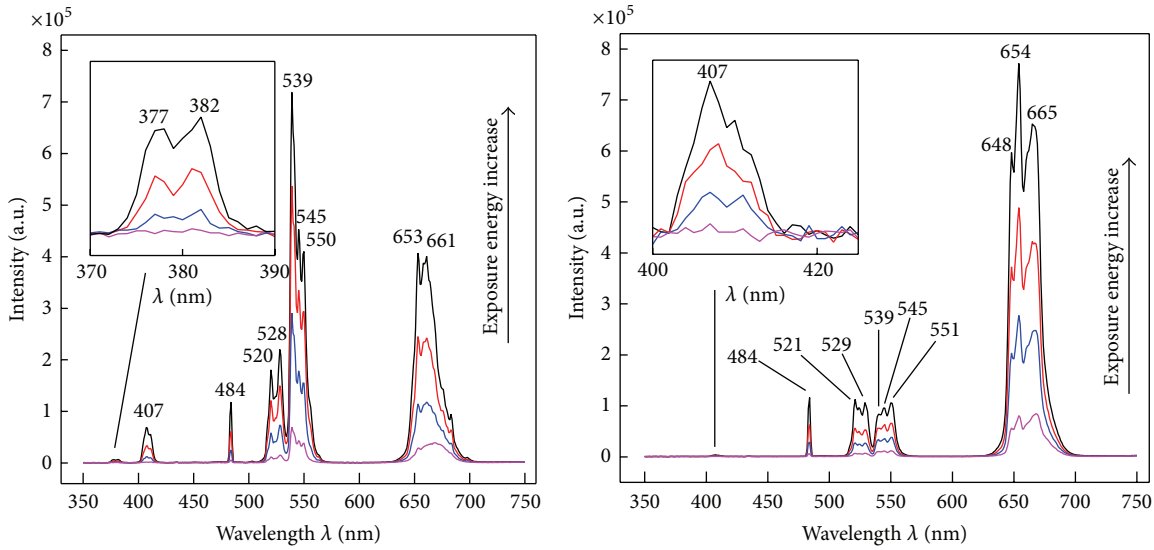

Figure 7: PL spectra of (a) Er^{3+} and (b) Er^{3+}/Yb^{3+} codoped nanocrystals when exposed to 980 nm laser.

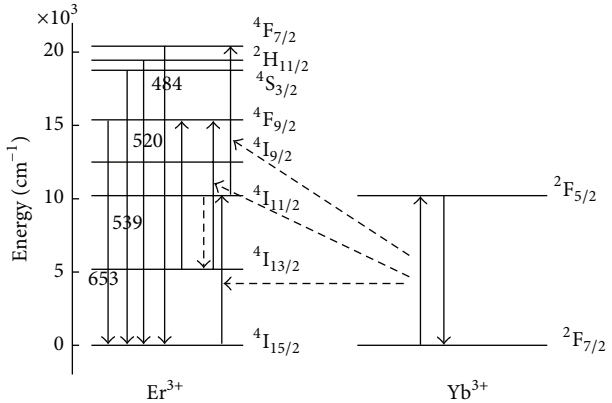

Figure 8: Schematic diagram illustrating the relative energy level of Er^{3+} and Yb^{3+}.

Table 1: Relationship between PL peak and Er^{3+} transition channel.

Peak λ/nm	Transition channel of Er^{3+}	Peak λ/nm	Transition channel of Er^{3+}
653, 661	$^4F_{9/2} \rightarrow {}^4I_{15/2}$	484	$^4F_{7/2} \rightarrow {}^4I_{15/2}$
539, 545, 550	$^4S_{3/2} \rightarrow {}^4I_{15/2}$	407	$^2H_{9/2} \rightarrow {}^4I_{15/2}$
520, 528	$^2H_{11/2} \rightarrow {}^4I_{15/2}$	380	$^4G_{11/2} \rightarrow {}^4I_{15/2}$

higher green luminance at 539 nm than red light at 653 nm appears for the only Er^{3+} doped material in Figure 7(a), and the red luminance at 654 nm has been remarkably enhanced and becomes higher than the green luminance around 539 nm after 0.5% Er^{3+} and 2% Yb^{3+} codoped, which is shown in Figure 7(b). This indicates that red light irradiation process of Er^{3+} ions has become the primary transition channel due to the Yb^{3+} codoping with Er^{3+} in $KZnF_3$ substrate.

The relative energy level state of Er^{3+} and Yb^{3+} is shown in Figure 8. According to Figure 8, the kind of emitting photon is determined by the occupied high energy level including $^4F_{7/2}(Er^{3+})$, $^2H_{11/2}(Er^{3+})$, $^4S_{3/2}(Er^{3+})$, and $^4F_{9/2}(Er^{3+})$, in which the $^2H_{11/2}(Er^{3+})$ and $^4S_{3/2}(Er^{3+})$ can be generated by nonradiative relaxation from $^4F_{7/2}(Er^{3+})$, and the $^4F_{9/2}(Er^{3+})$ is generated by energy relaxation from $^4S_{3/2}(Er^{3+})$, or relaxation from $^4I_{11/2}(Er^{3+})$ to $^4I_{13/2}(Er^{3+})$ and further access to $^4F_{9/2}(Er^{3+})$ by obtaining another 980 nm photon energy.

Consequently, the spontaneous emission occurs to emit one green photon or one red photon based on Mechanism 1 in Table 2. The multistep relaxation to $^4F_{9/2}(Er^{3+})$ has low quantum efficiency, and the red light of only Er^{3+} doped sample has relatively lower intensity compared to green light emission as seen in Figure 7(a). The major PL transition channel is $^4S_{3/2}(Er^{3+}) \rightarrow {}^4I_{15/2}(Er^{3+})$ after two-photon-exciting the only Er^{3+} doped sample.

Table 2: Sequential two-photon exciting upconversion transition channels for Er^{3+} doped or Er^{3+}/Yb^{3+} codoped nanocrystals.

Mechanism	Transition channel of Er^{3+} and Er^{3+}/Yb^{3+}	
Mechanism 1	$^4I_{15/2}(Er^{3+}) \xrightarrow{980\,nm} {}^4I_{11/2}(Er^{3+})$	
	$^4I_{11/2}(Er^{3+}) \xrightarrow{980\,nm} {}^4F_{7/2}(Er^{3+})$	
	$^4F_{7/2}(Er^{3+}) \rightarrow {}^4I_{15/2}(Er^{3+}) + \text{green light}$	484 nm
	$^4F_{7/2}(Er^{3+}) \xrightarrow{\text{energy relaxation}} {}^2H_{11/2}(Er^{3+})$	
	$\rightarrow {}^4I_{15/2}(Er^{3+}) + \text{green light}$	520 nm
	$^4F_{7/2}(Er^{3+}) \xrightarrow{\text{energy relaxation}} {}^4S_{3/2}(Er^{3+})$	
	$\rightarrow {}^4I_{15/2}(Er^{3+}) + \text{green light}$	539 nm
	$^4S_{3/2}(Er^{3+}) \xrightarrow{\text{energy relaxation}} {}^4F_{9/2}(Er^{3+})$	
	$\rightarrow {}^4I_{15/2}(Er^{3+}) + \text{red light}$	653 nm
	$^4I_{11/2}(Er^{3+}) \xrightarrow{\text{energy relaxation}} {}^4I_{13/2}(Er^{3+})$	
	$^4I_{13/2}(Er^{3+}) \xrightarrow{980\,nm} {}^4F_{9/2}(Er^{3+})$	
	$^4F_{9/2}(Er^{3+}) \rightarrow {}^4I_{15/2}(Er^{3+}) + \text{red light}$	653 nm
Mechanism 2	$^2F_{7/2}(Yb^{3+}) \xrightarrow{980\,nm} {}^2F_{5/2}(Yb^{3+})$	
	$^4I_{15/2}(Er^{3+}) + {}^2F_{5/2}(Yb^{3+}) \xrightarrow{\text{energy transfer}} {}^4I_{11/2}(Er^{3+}) + {}^2F_{7/2}(Yb^{3+})$	
	$^2F_{7/2}(Yb^{3+}) \xrightarrow{980\,nm} {}^2F_{5/2}(Yb^{3+})$	
	$^4I_{11/2}(Er^{3+}) + {}^2F_{5/2}(Yb^{3+}) \xrightarrow{\text{energy transfer}} {}^4F_{7/2}(Er^{3+}) + {}^2F_{7/2}(Yb^{3+})$	
	$\rightarrow {}^4I_{15/2}(Er^{3+}) + \text{green light}$	484 nm
	$^4F_{7/2}(Er^{3+}) \xrightarrow{\text{energy relaxation}} {}^2H_{11/2}(Er^{3+})$	
	$\rightarrow {}^4I_{15/2}(Er^{3+}) + \text{green light}$	520 nm
	$^4F_{7/2}(Er^{3+}) \xrightarrow{\text{energy relaxation}} {}^4S_{3/2}(Er^{3+})$	
	$\rightarrow {}^4I_{15/2}(Er^{3+}) + \text{green light}$	539 nm
	$^4S_{3/2}(Er^{3+}) \xrightarrow{\text{energy relaxation}} {}^4F_{9/2}(Er^{3+})$	
	$\rightarrow {}^4I_{15/2}(Er^{3+}) + \text{red light}$	653 nm
	$^4I_{11/2}(Er^{3+}) \xrightarrow{\text{energy relaxation}} {}^4I_{13/2}(Er^{3+})$	
	$^4I_{13/2}(Er^{3+}) + {}^2F_{5/2}(Yb^{3+}) \xrightarrow{\text{energy transfer}} {}^4F_{9/2}(Er^{3+}) + {}^2F_{7/2}(Yb^{3+})$	
	$^4F_{9/2}(Er^{3+}) \rightarrow {}^4I_{15/2}(Er^{3+}) + \text{red light}$	653 nm

In Er^{3+}/Yb^{3+} codoped nanocrystal, except that all the reactions in Mechanism 1 are taking place, the Yb^{3+} has also acted as sensitizer, which is shown in Mechanism 2. Yb^{3+} ion in $^2F_{5/2}(Yb^{3+})$ state can nonradiatively transfer the first absorbed 980 nm photon energy ($10.204 \times 10^3\ cm^{-1}$) and excited Er^{3+} from ground state $^4I_{15/2}(Er^{3+})$ to $^4I_{11/2}(Er^{3+})$, for which $^2F_{5/2}(Yb^{3+})$ and $^4I_{11/2}(Er^{3+})$ are at resonance level. Meanwhile, the Yb^{3+} ion returns to its ground state $^2F_{7/2}(Yb^{3+})$. Then, another energy transfer process can take place after $^2F_{7/2}(Yb^{3+})$ absorbs the second 980 nm photon, and the energy is transferred to excite Er^{3+} from $^4I_{11/2}(Er^{3+})$ to $^4F_{7/2}(Er^{3+})$ in order to further emit green and red upconversion photon according to the first part of Mechanism 2.

After Yb^{3+} was codoped with Er^{3+}, the enhanced red photon emitting from $^4F_{9/2}(Er^{3+})$ to $^4I_{15/2}(Er^{3+})$ can be ascribed to another procedure shown in the last part of Mechanism 2. The excited $^4I_{11/2}(Er^{3+})$ ions relax to metastable state $^4I_{13/2}(Er^{3+})$, and then the transferred energy from $^2F_{5/2}(Yb^{3+})$ excites $^4I_{13/2}(Er^{3+})$ to $^4F_{9/2}(Er^{3+})$ more efficiently. Therefore, remarkable enhancement of red emission appears in Figure 7(b), and the Yb^{3+} codoping with Er^{3+} has modified the transition channel of Er^{3+}, with the primary transition channel changing from $^4S_{3/2}(Er^{3+}) \rightarrow {}^4I_{15/2}(Er^{3+})$ to $^4F_{9/2}(Er^{3+}) \rightarrow {}^4I_{15/2}(Er^{3+})$. At the same time, the green emission channel has been suppressed in a given extent.

Also, it should be noticed that such transition channel after two-photon excitation does not change with exposure energy increasing in Figure 7, since the PL spectra curves under different exposure energies are similar.

Based on the above statement, it is obvious that the energy transfer from Yb^{3+} has modified PL emission of Er^{3+} from green light band to red band. And the energy transfer efficiency is depending on three factors. One is the matching energy levels between the two different kinds of ions; another is that the sensitizer has relatively big absorption cross section; the last is that Er^{3+} and Yb^{3+} ions must be near enough in crystal lattice.

4. Conclusion

Codoping Yb^{3+} with Er^{3+} in $KZnF_3$ cuboid perovskite type nanocrystal has been synthesized using hydrothermal method in this paper. Conclusions are presented as follows.

(1) After two-photon (980 nm) energy acquisition of the doped Er^{3+} ion, red emissions were derived from transition channel $^4F_{9/2} \rightarrow {}^4I_{15/2}$, green from $^4S_{3/2} \rightarrow {}^4I_{15/2}$, $^2H_{11/2} \rightarrow {}^4I_{15/2}$, and $^4F_{7/2} \rightarrow {}^4I_{15/2}$, and violet from $^2H_{9/2} \rightarrow {}^4I_{15/2}$. And the major transition channel is $^4S_{3/2}(Er^{3+}) \rightarrow {}^4I_{15/2}(Er^{3+})$ of the only Er^{3+} doped $KZnF_3$ sample.

(2) Modification of upconversion photoluminescence (PL) of Er^{3+}, changed from green light band to red band, has been achieved by Yb^{3+} codoped with Er^{3+}. The red photon emitting has been remarkably intensified compared to only Er^{3+} doped $KZnF_3$ nanocrystal. The major transition channel has changed to $^4F_{9/2}(Er^{3+}) \rightarrow {}^4I_{15/2}(Er^{3+})$ of the Er^{3+}/Yb^{3+} codoped sample.

(3) The mechanism of the modification has been discussed in which the excited $^4I_{11/2}(Er^{3+})$ state relaxes to metastable state $^4I_{13/2}(Er^{3+})$, and then the transferred energy from $^2F_{5/2}(Yb^{3+})$ efficiently excites $^4I_{13/2}(Er^{3+})$ to $^4F_{9/2}(Er^{3+})$. In such two-photon upconversion process, the Yb^{3+} has acted as sensitizer, not only for its higher absorption section than Er^{3+}, but also for its high energy transfer efficiency.

Such upconversion nanocrystals can be applied as luminescent probes in biological labeling and imaging technology. Results obtained in this paper can be used for rare earth doping for spectrum conversion, in order to improve the display efficiency.

Conflict of Interests

The authors declare that there is no conflict of interests regarding the publication of this paper.

Acknowledgments

This work is financially supported by the Specialized Research Fund for the Doctoral Program of Higher Education 20101301120002, International Foundation for Science C4690, and the Natural Science Foundation of Hebei Province F2011201103.

References

[1] A. Splendiani, L. Sun, Y. Zhang et al., "Emerging photoluminescence in monolayer MoS_2," *Nano Letters*, vol. 10, no. 4, pp. 1271–1275, 2010.

[2] P. Peng, W. D. Zhang, H. Q. He, R. H. Liu, Y. S. Hu, and X. L. Ma, "Luminescence properties of oxyfluoride phosphor $Sr_{2.975-x}Ca_xAlO_4F:Ce^{3+}_{0.025}$ for UV-LEDs," *Journal of the Chinese Society of Rare Earths*, vol. 31, no. 4, p. 414, 2013 (Chinese).

[3] R. Kumar, M. Nyk, T. Y. Ohulchanskyy, C. A. Flask, and P. N. Prasad, "Combined optical and MR bioimaging using rare earth ion doped $NaYF_4$ nanocrystals," *Advanced Functional Materials*, vol. 19, no. 6, pp. 853–859, 2009.

[4] H. Y. Ni, H. B. Liang, C. M. Liu, Q. Su, and G. B. Zhang, "Luminescence of Ce^{3+} ion activated sodium gadolinium pyrosilicates phosphor under vacuum ultraviolet-vis excitation," *Journal of the Chinese Rare Earth Society*, vol. 31, no. 1, pp. 38–43, 2013 (Chinese).

[5] J. Wang, J. H. Hao, and P. A. Tanner, "Luminous and tunable white-light upconversion for YAG ($Yb_3Al_5O_{12}$) and $(Yb, Y)_2O_3$ nanopowders," *Optics Letters*, vol. 35, no. 23, pp. 3922–3924, 2010.

[6] H. T. Wong, M. K. Tsang, C. F. Chan, K. L. Wong, B. Fei, and J. Hao, "In vitro cell imaging using multifunctional small sized $KGdF_4:Yb^{3+},Er^{3+}$ upconverting nanoparticles synthesized by a one-pot solvothermal process," *Nanoscale*, vol. 5, no. 8, pp. 3465–3473, 2013.

[7] H. L. Qiu, G. Y. Chen, R. W. Fan et al., "Intense ultraviolet upconversion emission from water-dispersed colloidal $YF_3:Yb^{3+}/Tm^{3+}$ rhombic nanodisks," *Nanoscale*, vol. 6, no. 2, pp. 753–757, 2013.

[8] F. Wang, Y. Han, C. S. Lim et al., "Simultaneous phase and size control of upconversion nanocrystals through lanthanide doping," *Nature*, vol. 463, no. 7284, pp. 1061–1065, 2010.

[9] S. Obregón and G. Colón, "Evidence of upconversion luminescence contribution to the improved photoactivity of erbium doped TiO_2 systems," *Chemical Communications*, vol. 48, no. 63, pp. 7865–7867, 2012.

[10] F. Xin, S. Zhao, L. Huang et al., "Up-conversion luminescence of Er^{3+}-doped glass ceramics containing β-$NaGdF_4$ nanocrystals for silicon solar cells," *Materials Letters*, vol. 78, pp. 75–77, 2012.

[11] F. Auzel, "Upconversion and anti-stokes processes with f and d ions in solids," *Chemical Reviews*, vol. 104, no. 1, pp. 139–173, 2004.

[12] T. Aisaka, M. Fujii, and S. Hayashi, "Enhancement of upconversion luminescence of Er doped Al_2O_3 films by Ag island films," *Applied Physics Letters*, vol. 92, no. 13, Article ID 132105, 2008.

[13] W. H. Zhang, F. Ding, and S. Y. Chou, "Large enhancement of upconversion luminescence of $NaYF_4:Yb^{3+}/Er^{3+}$ nanocrystal by 3D plasmonic nanoantennas," *Advanced Materials*, vol. 24, no. 35, pp. OP236–OP241, 2012.

[14] F. Vetrone, R. Naccache, V. Mahalingam, C. G. Morgan, and J. A. Capobianco, "The active-core/active-shell approach: a strategy to enhance the upconversion luminescence in lanthanide-doped nanoparticles," *Advanced Functional Materials*, vol. 19, no. 18, pp. 2924–2929, 2009.

[15] C. Zhang, P. A. Ma, C. Li et al., "Controllable and white upconversion luminescence in $BaYF_5:Ln^{3+}$ (Ln = Yb, Er, Tm) nanocrystals," *Journal of Materials Chemistry*, vol. 21, no. 3, pp. 717–723, 2011.

[16] G. Phaomei and W. R. Singh, "Effect of solvent on luminescence properties of re-dispersible $LaF_3:Ln^{3+}$ (Ln^{3+}=Eu^{3+}, Dy^{3+}, Sm^{3+} and Tb^{3+}) nanoparticles," *Journal of Rare Earths*, vol. 31, no. 4, pp. 347–355, 2013.

[17] G. Tian, Z. Gu, L. Zhou et al., "Mn^{2+} dopant-controlled synthesis of $NaYF_4$:Yb/Er upconversion nanoparticles for in vivo imaging and drug delivery," *Advanced Materials*, vol. 24, no. 9, pp. 1226–1231, 2012.

[18] X. A. Zhang, S. G. Xiao, X. L. Yang, and X. L. Jin, "Enhanced red emission in Eu^{3+} doped fluoro-borosilicate glass by introducing ZnF_2," *Journal of Optoelectronics and Advanced Materials*, vol. 15, no. 9-10, pp. 971–975, 2013.